FARADAY

Chiral induction in nematics

A computer simulation study

Roberto Berardi,[a] Hans-Georg Kuball,[b] Reiner Memmer[b] and Claudio Zannoni[a]

[a] *Dipartimento di Chimica Fisica ed Inorganica, Università, Viale Risorgimento 4, 40136 Bologna, Italy*

[b] *Fachbereich Chemie, Universität Kaiserslautern, Erwin–Schrödinger–Strasse, 67663 Kaiserslautern, Germany*

We have studied chiral induction in a nematic in contact with a chiral surface using computer simulations. Nematic and surface particles have been modelled using the Gay–Berne (GB) potential considering, additionally, a short-range chiral term for the inducing surface. We find that, close to the chiral surface, a twist of the local director with respect to the surface molecules is induced, even in the isotropic phase. In the nematic phase, the twist is maintained through orientational correlation and, even well inside, the sample molecules are effectively twisted with respect to the surface director. This process can highlight the basic mechanism of the chiral induction of a cholesteric, *i.e.* chiral nematic, phase. A detailed description of the molecular organization at various distances from the inducing surface is presented, using scalar and pseudoscalar orientational correlation functions.

A well known but still fascinating effect is the induction of a chiral nematic phase upon dissolving a small quantity of a chiral solute in a nematic,[1,2] which can exhibit a huge susceptivity to this chiral perturbation. Such induced chiral nematic phases have a helical structure with a repeat distance that can be of a length comparable to the wavelength of visible or IR light, depending on solute–solvent characteristics and solute concentration. The induction of a macroscopic twist seems likely to be connected to the extent of orientational pair correlation. In fact, the induced optical activity, which is a measurable quantity related to chirality, is very weak in the isotropic phase compared to that measurable in nematic phases.[3,4] Since the concentration of chiral dopants needed to induce a cholesteric phase can be very low, even mole fractions of the chiral inducer below 10^{-4} are sufficient,[5] it is difficult to understand how the local director twist is generated and propagated. Indeed, every chiral molecule is expected to have an environment with a large predominance of achiral molecules and yet the chiral induction is very effective. This is further complicated by the fact that chiral interactions are expected to be, on one hand, weak and, on the other, fairly short-ranged.[6,7] The induction of a chiral nematic phase has been extensively studied, both experimentally and theoretically (see *e.g.* ref. 8 and references therein). However, we are aware of no detailed computer simulation study of systems of chiral molecules dissolved in a nematic phase. Such a study would, in any case, be very complicated, using computer simulations, particularly since the low concentrations involved would make it very difficult to calculate meaningful statistics.

We have thus decided to study by computer simulation the chiral induction in a simpler and more controlled system, where a nematic is put in contact with a surface covered by chiral molecules which cannot diffuse into the nematic bulk. Such systems could be prepared by coating the surface in contact with the nematic with a layer of chiral molecules or with a chiral polymer.

In this work we investigate such a system setting up a GB-based model described in the next section. We shall also quantify the extent of twist and spatial correlation by introducing a relevant set of scalar and pseudoscalar orientational correlation functions. The model will then be studied in detail using Monte Carlo computer simulation and the results will be discussed in the final section.

Model system

Our aim is to study how chirality is propagated from a suitably prepared chiral surface to a nematic with which it is in contact. To do this we have to choose a model nematic and enclose it in a simulation box with a chiral wall. As a model for the nematic we have employed a set of elongated ellipsoidal molecules interacting with the GB potential

$$U_{\mathrm{GB}} = 4\varepsilon_0 \frac{\varepsilon'^{\mu}(\hat{\boldsymbol{u}}_i, \hat{\boldsymbol{u}}_j, \hat{\boldsymbol{r}})}{\{1 - \kappa^2(\hat{\boldsymbol{u}}_i \cdot \hat{\boldsymbol{u}}_j)^2\}^{\nu/2}} \times \left[\left\{\frac{\sigma_{\mathrm{s}}}{r - \sigma(\hat{\boldsymbol{u}}_i, \hat{\boldsymbol{u}}_j, \hat{\boldsymbol{r}}) + \sigma_{\mathrm{s}}}\right\}^{12} - \left\{\frac{\sigma_{\mathrm{s}}}{r - \sigma(\hat{\boldsymbol{u}}_i, \hat{\boldsymbol{u}}_j, \hat{\boldsymbol{r}}) + \sigma_{\mathrm{s}}}\right\}^{6}\right] \quad (1)$$

where the anisotropic terms $\sigma(\hat{\boldsymbol{u}}_i, \hat{\boldsymbol{u}}_j, \hat{\boldsymbol{r}})$ and $\varepsilon'(\hat{\boldsymbol{u}}_i, \hat{\boldsymbol{u}}_j, \hat{\boldsymbol{r}})$ are related to molecular shape and well-depth as described in detail in ref. 9 and 10. The unit vectors $\hat{\boldsymbol{u}}_i, \hat{\boldsymbol{u}}_j$ [where $\hat{\boldsymbol{u}}_i \equiv (u_{xi}, u_{yi}, u_{zi})$] describe the orientation of the long axis of particles i, j, with position $\boldsymbol{r}_i \equiv (x_i, y_i, z_i)$ in the laboratory frame. $\boldsymbol{r} = \boldsymbol{r}_j - \boldsymbol{r}_i \equiv (r_x, r_y, r_z)$ is the intermolecular vector (of length r and associated unit vector $\hat{\boldsymbol{r}}$). σ_{s} and ε_0 are taken as units for distances and energies. This generalized anisotropic Lennard-Jones (LJ) interaction depends on a few parameters: length-to-breadth ratio of the molecules $\kappa \equiv \sigma_{\mathrm{e}}/\sigma_{\mathrm{s}}$, side-by-side to end-to-end interaction strength ratio $\kappa' \equiv \varepsilon_{\mathrm{s}}/\varepsilon_{\mathrm{e}}$ and the two additional adjustable parameters μ, ν that can be chosen to fit a specific type of molecular model and that, ultimately, modify the GB phase diagram obtained. In the original formulation[9,11] $\kappa = 3$, $\kappa' = 5$, $\mu = 2$ and $\nu = 1$ were chosen to fit the intermolecular potential of a linear array of four closely spaced LJ spherical sites. However, this choice, that has the advantage of being extensively studied, tends to give a rather narrow nematic range.[12,13] We have thus used the parametrization[10] $\kappa = 3$, $\kappa' = 5$, $\mu = 1$ and $\nu = 3$, recently also studied in ref. 14, that we have shown to give a wide nematic range (between scaled temperatures $T^*_{\mathrm{SN}} \approx 2.2$ and $T^*_{\mathrm{NI}} \approx 3.55$, where $T^* \equiv k_{\mathrm{B}}T/\varepsilon_0$) and a temperature dependence of the second rank order parameter $\langle P_2 \rangle$[15] that resembles more closely the experimental one for molecules such as cyanobiphenyls, *n*-(4 methoxybenzylidene)-4′-*n*-butylaniline (MBBA) and other nematogens.

A system of N such particles will be studied in an elongated box with volume V and sides L_x, L_y and L_z using periodic

boundary conditions around the x and y sides and confined at the top and bottom by a wall of GB particles, with the addition of a chiral contribution for the particles at the bottom. In this way we avoid the artifact of a continuum surface wall and we can use a similar potential for the interaction between fluid molecules and fluid-surface in an effort to reduce the spurious effects that can be caused by the inevitably small size of the sample. We have chosen to use only one chiral surface, in order to avoid any superposition with additional chiral induction effects. Moreover, a fairly large $L_z^* \equiv L_z/\sigma_s$ side of the simulation box has been chosen to minimize the effects of interactions of fluid particles with both surfaces and to have a central fluid region that is, on the one hand, relatively broad and, on the other, well separated from the boundaries. The boundary walls are referred as the 'chiral surface' (bottom) and the 'achiral surface' (top). The pair interaction between fluid particles and chiral surface molecules is given by $U = U_{GB} + cU_{ch}$, where the chiral interaction term is[6,7,16]

$$U_{ch} = -4\sqrt{\frac{10}{3}}\,\varepsilon_0 \frac{\varepsilon'^{\mu}(\hat{\boldsymbol{u}}_i, \hat{\boldsymbol{u}}_j, \hat{\boldsymbol{r}})}{[1-\kappa^2(\hat{\boldsymbol{u}}_i \cdot \hat{\boldsymbol{u}}_j)^2]^{\nu/2}} \times \left\{\frac{\sigma_s}{r - \sigma(\hat{\boldsymbol{u}}_i, \hat{\boldsymbol{u}}_j, \hat{\boldsymbol{r}}) + \sigma_s}\right\}^7 S^{221}(\hat{\boldsymbol{u}}_i, \hat{\boldsymbol{u}}_j, \hat{\boldsymbol{r}}) \quad (2)$$

which contains the chiral rotational invariant[17]

$$S^{221}(\hat{\boldsymbol{u}}_i, \hat{\boldsymbol{u}}_j, \hat{\boldsymbol{r}}) = -\sqrt{\frac{3}{10}}\,(\hat{\boldsymbol{u}}_i \cdot \hat{\boldsymbol{u}}_j \times \hat{\boldsymbol{r}})(\hat{\boldsymbol{u}}_i \cdot \hat{\boldsymbol{u}}_j) \quad (3)$$

The pseudoscalar parameter c, for convenience denoted as chirality parameter, determines the strength of the chiral interaction between chiral surface molecules and fluid particles, and it changes sign under reflection, as $S^{221}(\hat{\boldsymbol{u}}_i, \hat{\boldsymbol{u}}_j, \hat{\boldsymbol{r}})$, giving an overall scalar interaction potential. We have chosen, for the shifted distance dependence of the chiral term, a functional form similar to that of the attractive and repulsive contributions to the GB potential but with an inverse seventh power dependence as often assumed for chiral interactions.[6,7,16] Such a model system allows us to study the combined effect of anisotropic GB interactions between fluid particles and the short-range chiral interactions affecting molecules in proximity of the chiral surface.

We have used a chirality parameter $c = -2$ and show in Fig. 1 the distance dependence for the most favourable twisted side-by-side interaction energy $U^* \equiv U/\varepsilon_0$ between a chiral surface molecule parallel to the y axis and a fluid particle, with both centres of mass positioned along the z axis. The long axis $\hat{\boldsymbol{u}}_i$, of the mesogenic particle was constrained parallel to the xy plane and the twist angle θ with respect to the surface molecule was then varied until the most attractive interaction was found. Comparing this curve with the energy profile for a fixed $\theta = 45°$ twist and the energy for the side-by-side ($\theta = 0°$) configuration we see that, even for the most favourable configuration, the contribution of the chiral energy to the total interaction is relevant only for small intermolecular distances r. In practice, the effective range of the chiral energy term cU_{ch} is comparable with one molecular diameter σ_s and the chiral interaction of fluid molecules with the inducing surface does not extend beyond the first or second shell of surface neighbours.

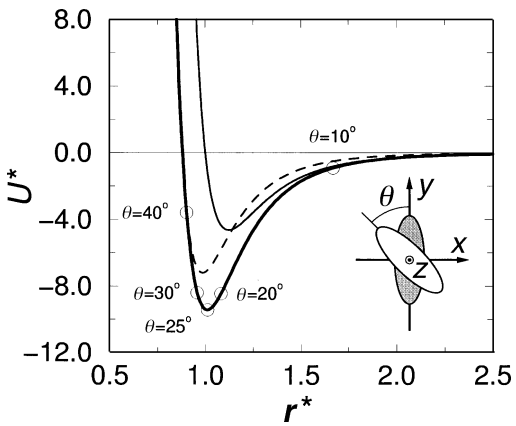

Fig. 1 Most favourable twisted side-by-side interaction energy (thick curve) between a chiral surface molecule (light grey) and a fluid particle (white) with both centres of mass positioned along the z axis. For each separation r^*, the twist angle θ was optimized in order to give the most attractive interaction energy $U^* \equiv U/\varepsilon_0 = U^*_{GB} + cU^*_{ch}$ while keeping the long axis of the fluid particle parallel to the xy plane. The optimized twist angle θ is reported for a few selected distances. The energy for the side-by-side configuration ($\theta = 0°$) (thin curve), and for a fixed $\theta = 45°$ twist (dashed curve) are reported for comparison.

Structural properties

In order to characterize and quantify the chiral induction we need to introduce a set of observables that describe the orientational correlation of fluid molecules amongst themselves and, more importantly in this case, with the chiral molecules anchored at the basal surface. A general way of doing this is to consider averages of a suitable subset of the rotational invariant functions $S^{L_1L_2L_3}(\hat{\boldsymbol{u}}_i, \hat{\boldsymbol{u}}_j, \hat{\boldsymbol{r}})$ introduced by Stone.[17] The averages can be defined as integrals with respect to all orientational variables of the function of interest at a given intermolecular separation over the pair distribution function

$$S^{L_1L_2L_3}(\boldsymbol{r}_1, \boldsymbol{r}_2) = \frac{1}{\rho^2}\int \mathrm{d}\hat{\boldsymbol{u}}_1\,\mathrm{d}\hat{\boldsymbol{u}}_2\,P^{(2)}(\boldsymbol{r}_1, \hat{\boldsymbol{u}}_1, \boldsymbol{r}_2, \hat{\boldsymbol{u}}_2)S^{L_1L_2L_3}(\hat{\boldsymbol{u}}_1, \hat{\boldsymbol{u}}_2, \hat{\boldsymbol{r}}) \quad (4)$$

$$= \frac{1}{\rho^2}\langle\delta(\boldsymbol{r}_i - \boldsymbol{r}_1)\,\delta(\boldsymbol{r}_j - \boldsymbol{r}_2)S^{L_1L_2L_3}(\hat{\boldsymbol{u}}_1, \hat{\boldsymbol{u}}_2, \hat{\boldsymbol{r}})\rangle_{ij} \quad (5)$$

where $\rho = N/V$ is the number density, $P^{(2)}(\boldsymbol{r}_1, \hat{\boldsymbol{u}}_1, \boldsymbol{r}_2, \hat{\boldsymbol{u}}_2)$ is the pair distribution function, and $\langle\ldots\rangle_{ij}$ represents an ensemble average with respect to all molecular pairs. Considering the geometry of the confined system, it is convenient to treat the fluid sample as a collection of virtual planar slabs parallel to the xy plane and identified by the z coordinates of their centres. Thus we can concentrate on average invariants of the type

$$S^{L_1L_2L_3}(z_1, z_2) = \frac{1}{(L_x L_y \rho)^2}\int \mathrm{d}x_1\,\mathrm{d}y_1\,\mathrm{d}\hat{\boldsymbol{u}}_1\,\mathrm{d}x_2\,\mathrm{d}y_2\,\mathrm{d}\hat{\boldsymbol{u}}_2 \times P^{(2)}(\boldsymbol{r}_1, \hat{\boldsymbol{u}}_1, \boldsymbol{r}_2, \hat{\boldsymbol{u}}_2)S^{L_1L_2L_3}(\hat{\boldsymbol{u}}_1, \hat{\boldsymbol{u}}_2, \hat{\boldsymbol{r}}_z) \quad (6)$$

$$= \frac{1}{(L_x L_y \rho)^2}\langle\delta(z_i - z_1)\,\delta(z_j - z_2) \times S^{L_1L_2L_3}(\hat{\boldsymbol{u}}_1, \hat{\boldsymbol{u}}_2, \hat{\boldsymbol{r}}_z)\rangle_{ij} \quad (7)$$

where $\hat{\boldsymbol{r}}_z = (0, 0, r_z/|r_z|)$ is the normalized projection of the intermolecular vector $\boldsymbol{r}$ along the laboratory z axis. These correlation functions are calculated as histograms during the MC runs performing averages over all pairs of particles in the simulation box belonging to the appropriate bins along z. In particular, we have computed the fluid–fluid orientational pair correlation functions

$$S^{220}(z_1, z_2) = \frac{1}{2\sqrt{5}(L_x L_y \rho)^2} \times \langle\delta(z_i - z_1)\,\delta(z_j - z_2) \times [3(\hat{\boldsymbol{u}}_i \cdot \hat{\boldsymbol{u}}_j)^2 - 1]\rangle_{ij} \quad (8)$$

which express the average second-rank order of molecules at z_1 with respect to those at z_2, and the simplest chiral corre-

lation

$$S^{221}(z_1, z_2) = -\frac{\sqrt{3}}{\sqrt{10}(L_x L_y \rho)^2} \times \langle \delta(z_i - z_1)\, \delta(z_j - z_2) \times (\hat{\boldsymbol{u}}_i \cdot \hat{\boldsymbol{u}}_j \times \hat{\boldsymbol{r}}_z)(\hat{\boldsymbol{u}}_i \cdot \hat{\boldsymbol{u}}_j)\rangle_{ij} \quad (9)$$

The functions $S^{220}(z_1, z_2)$ and $S^{221}(z_1, z_2)$ describe the principal orientational and chiral correlation between pairs of fluid molecules whose centres of mass are at distance z_1 and z_2 from the chiral surface. It is worth noticing that the second function is related to the chiral interaction term U_{ch}. Using $z_1 = 0$, the correlation functions reduce to those between chiral surface particles and fluid molecules, which we shall simply indicate as $S^{L_1L_2L_3}(z) \equiv S^{L_1L_2L_3}(0, z)$. Since all boundary molecules are parallel, it is possible to integrate with respect to this Dirac's delta distribution of angular variables. We have thus computed the chiral surface–fluid correlation functions

$$g_0(z) \equiv S^{000}(z) = \frac{1}{L_x L_y \rho} \langle \delta(z_i - z)\rangle_i \quad (10)$$

$$S^{022}(z) = \frac{1}{2\sqrt{5} L_x L_y \rho} \langle \delta(z_i - z)(3u_{zi}^2 - 1)\rangle_i \quad (11)$$

and

$$S^{221}(z) = \frac{\sqrt{3}}{\sqrt{10} L_x L_y \rho} \langle \delta(z_i - z) u_{xi} u_{yi}\rangle_i \quad (12)$$

where $\langle \ldots \rangle_i$ represents an ensemble average with respect to all fluid particles. $g_0(z)$ is the density distribution function along z. The histogram $S^{022}(z)$ measures the average tilt of fluid particles outside the xy plane, while $S^{221}(z)$ quantifies the principal chiral correlation between chiral particles and fluid molecules at distance z.

Computer simulations and discussion

We have investigated this confined fluid model system employing Monte Carlo[15] computer simulations in the canonical ensemble using an overall cut-off radius for the pair potential $r_c^* = r_c/\sigma_s = 4.0$ at a density $\rho^* \equiv \sigma_s^3 \rho = \sigma_s^3 N/V = 0.30$ where N is the number of particles and $V = L_x L_y L_z$ is the sample volume. We have used a box containing $N = 2048$ particles with sides $L_x^* \equiv L_x/\sigma_s = 16$, $L_y^* \equiv L_y/\sigma_s = 12$ and $L_z^* \equiv L_z/\sigma_s = 35.56$. The two layers of surface particles are parallel to the xy plane and are centred, respectively, at $z^* = 0$ (chiral surface), $z^* = 35.56$ (achiral surface). Each layer is formed by $N_s = 64$ GB molecules aligned to the y axis and arranged along x as 16 adjacent columns of 4 end-to-end particles. Neighbouring columns are translated in the y direction by half molecular length σ_e, *i.e.* the distribution of centres of surface particles is that of a two-dimensional hexagonal lattice. Positions and orientations of surface particles are kept fixed during the simulation and define the boundaries along the z direction, while for both x and y directions periodic boundary conditions have been used. We have updated the sample using the standard Metropolis procedure moving one randomly selected particle at a time. Orientations were randomly sampled using the Barker–Watts method[18] and the sampling ranges chosen to guarantee an overall acceptance ratio of 0.5.

We have divided the range $[0, L_z^*]$ for the z^* coordinate in 200 histogram bins so that on average each bin contains 10 fluid molecules. To reduce the statistical noise of the averaged histograms it was necessary to perform long production runs. We have examined five temperatures equally distributed between $T^* = 4.0$ and $T^* = 3.2$ using typically 4×10^5 cycles for the equilibration and 6×10^5 cycles for the production runs, where a cycle is a sequence of N attempted MC particle moves.

In Fig. 2 we report the average total energy per particle of the confined fluid $\langle U^* \rangle \equiv \langle U \rangle/\varepsilon_0$ as a function of temperature and compare it with that of an unconfined GB bulk system of $N = 1000$ particles with periodic boundary conditions applied in x, y and z directions with the same parametrization and number density.[10] At $T^* = 3.4$ this bulk system forms a nematic phase with second-rank orientational order parameter $\langle P_2 \rangle = 0.63$, which increases to $\langle P_2 \rangle = 0.72$ at $T^* = 3.2$. The confined system is already orientationally ordered at $T^* = 3.6$ owing to the effect of the aligned walls. In addition, in Fig. 2 we plot the average GB energy per particle restricted to interactions between fluid particles $\langle U_{GB}^* \rangle_f$. The average molecular energy due to surface–fluid interactions, which is the difference $\langle U^* \rangle - \langle U_{GB}^* \rangle_f$, is almost independent of temperature. We now turn to the local structural properties at different temperatures. In Fig. 3 we report the profiles across the sample of the density distribution $g_0(z^*)$, of the principal orientational fluid–fluid correlation function for particles within the same slab $S^{220}(z^*, z^*)$, and of the xy off-plane tilt correlation $S^{022}(z^*)$ at temperatures $T^* = 4.0$ and $T^* = 3.2$. The estimated root-mean-squared fluctuations are shown as well.

We notice that, at high temperature, when the confined fluid is isotropic, both $S^{220}(z^*, z^*)$ and $S^{022}(z^*)$ are very close to zero, except for the narrow fluid regions in the proximity of the boundaries, where surface effects are stronger and the molecules fairly well aligned. From the close spacing of the near-surface peaks in the density profile $g_0(z^*)$, we see that these small regions have a two-dimensional distribution of the centres of mass, with the molecules arranged in layers parallel to the xy plane. The extension of these structured regions is limited to *ca.* 3 molecular diameters σ_s at all temperatures studied, while the overwhelming part of the sample is a homogeneous fluid $[g_0(z^*) \approx 1]$.

At the lowest temperature studied, $T^* = 3.2$ (Fig. 3), the function $S^{022}(z^*)$ is close to its minimum value $[S^{022}(z^*)]_{min} = -1/2\sqrt{5} \approx -0.224$, which means that the molecular axes $\hat{\boldsymbol{u}}_i$ are essentially parallel to the xy plane. The histogram $S^{220}(z^*, z^*)$ is uniform and symmetric with respect to the central slab at $z^* = L_z^*/2$, showing that, within the fluid phase, the local orientational order is uniformly distributed, independent of the actual orientation of the local director. Only in the proximity of the surfaces does the degree of alignment increase further, approaching the maximum value

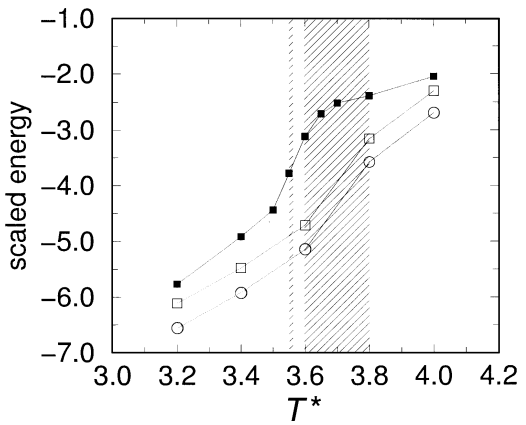

Fig. 2 Temperature dependence of the average total energy per fluid molecule $\langle U^* \rangle$ (○), the $\langle U_{GB}^* \rangle_f$ energy per particle due to fluid–fluid interactions (□), and the temperature range embracing the N–I transition of the confined fluid system (hatched band). The GB energy profile (■) for the unconfined bulk system[10] in the same temperature range and the N–I transition ($T_{NI}^* = 3.55$, hatched line), are reported for comparison.

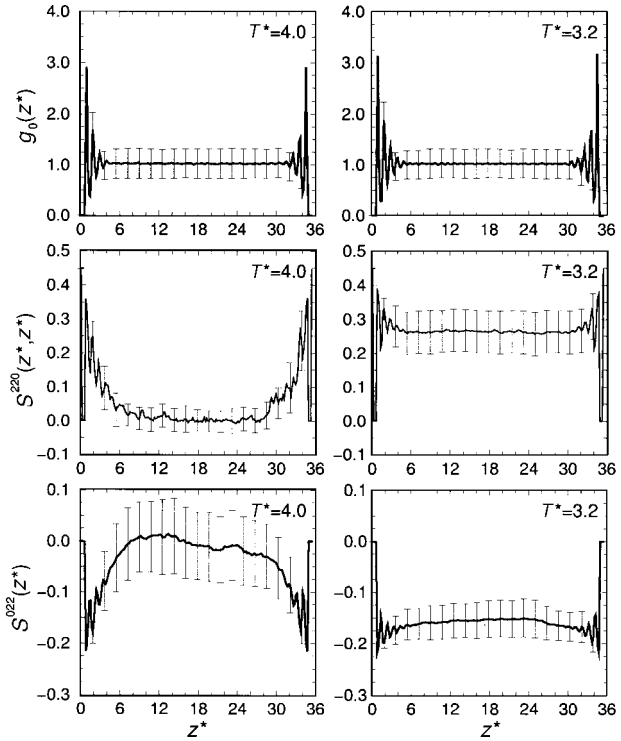

Fig. 3 Density distribution function $g_0(z^*)$ (top), principal orientational correlation for fluid particles within the same slab $S^{220}(z^*, z^*)$ (middle), and xy off-plane tilt correlation $S^{022}(z^*)$ (bottom) for the temperatures $T^* = 4.0$ (left) and $T^* = 3.2$ (right). The estimated root-mean-squared fluctuations are plotted every twenty bins.

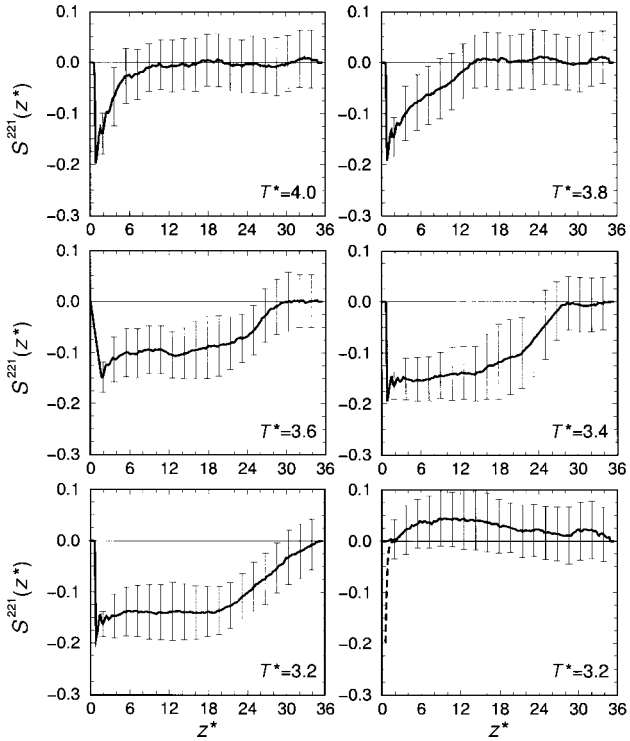

Fig. 4 Chiral correlation $S^{221}(z^*)$ and its root-mean-squared fluctuation (plotted every twenty bins) for the five temperatures studied. Additionally, the $S^{221}(z^*)$ for a system confined between two achiral surfaces ($c = 0$, continuous line), and for the approximate model described in the text (dashed line) are shown for $T^* = 3.2$ in the bottom right-hand diagram.

$[S^{220}(z^*, z^*)]_{max} = 1/\sqrt{5} \approx 0.447$. The central portion of the sample is still uniform, as shown by the density profile $g_0(z^*)$.

To quantify the induced twist of the local director we have plotted $S^{221}(z^*)$ for the five temperatures studied (Fig. 4). We observe that while no twist appears on the achiral surface side at all temperatures, the induced twist of the director propagates from the chiral surface well inside the fluid phase. This effect consists in a right-handed twist of the local director with respect to the laboratory y axis, as indicated by the negative sign of the $S^{221}(z^*)$ function. The thickness of the twisted region changes with temperature, and the relaxation length increases with the local orientational ordering of the fluid. At high temperatures the $S^{221}(z^*)$ drops rapidly to zero as we move away from the chiral surface at $z^* = 0$. However, even at temperatures $T^* = 4.0$ and $T^* = 3.8$, in spite of the central portion of the sample being isotropic, the director relaxation range still extends for over 6–12 molecular diameters σ_s. On lowering the temperature to $T^* = 3.6$, the whole sample becomes aligned and the chiral-induced twist of the local director moves further into the fluid region, almost doubling its range. At this temperature the bulk system[10] is still isotropic, slightly above the N–I transition. At the lowest temperatures the range of the chiral surface–fluid correlation $S^{221}(z^*)$ is further extended and, at $T^* = 3.2$, its slow decrease makes it significant, even in proximity to the achiral surface. This behaviour is different from that observed in computer simulations of cholesteric phases of pure systems of chiral molecules[16] or that obtained using twisted boundary conditions[19–21] where the local director varies uniformly in space along the helical axis. To determine if the information provided by these correlation functions is truly significant, we have compared these profiles with those obtained studying a similar reference system where both surfaces are achiral ($c = 0$) and that has been thoroughly equilibrated at the same temperature for a comparable number of cycles. The correlation function $S^{221}(z^*)$ for this reference system at $T^* = 3.2$ is also plotted in Fig. 4 (bottom right-hand diagram). We see that no twist is observed within the precision of the computer experiment, confirming that the effects observed are not due to the finite sample size or to other spurious simulation flukes.

To have a cross-check that the chiral induction is not arising only on the basis of direct chiral surface–fluid molecule interactions, we have computed, at $T^* = 3.2$, the dependence of the chiral correlation function $S^{221}(z^*)$ for an approximate two-particle model system formed by a chiral surface and an achiral fluid molecule positioned at $\boldsymbol{r}^* = (0, 0, z^*)$. The averaging is performed with respect to the orientational distribution for the fluid particle $P(\hat{\boldsymbol{u}}_i, z^*) \propto \exp[-U^*(\hat{\boldsymbol{u}}_i, z^*)/T^*]$. In Fig. 4 we plot the chiral correlation function for this two-particle model system, and we see that it goes very rapidly to zero (roughly in two molecular diameters) well before reaching the potential cut-off radius r_c^*.

In Fig. 5 we show, for the system at $T^* = 3.2$, the fluid–fluid chiral correlation functions $S^{221}(z_0^*, z^*)$ between reference particles at selected distances z_0^* and those in the rest of the sample. These functions measure the chiral correlation between fluid slabs by considering explicitly the orientation of all pairs of molecules belonging to two regions of the sample. We have considered two cases, with the reference slabs chosen in regions either close to the chiral ($z_0^* = 7.1$) or achiral ($z_0^* = 28.4$) surfaces, but at a distance larger than the potential cut-off radius r_c^*. In the first case, the function is almost zero around the reference slab, showing that the fluid–fluid chiral correlation does not change over the wide range of the fluid sample where the local director has an almost constant twist θ with respect to y. In the second case the correlation function is changing its magnitude around $z_0^* = 28.4$ showing that, in this fluid region, the local director is relaxing back to a direction parallel to y, which can be understood as a result of the influence of the achiral surface. The local director relaxation is left-handed, as shown by the positive sign of the $S^{221}(z_0^*, z^*)$ function. Additionally, this analysis shows that there are no regions close to the chiral surface where the $S^{221}(z_0^*, z^*)$ corre-

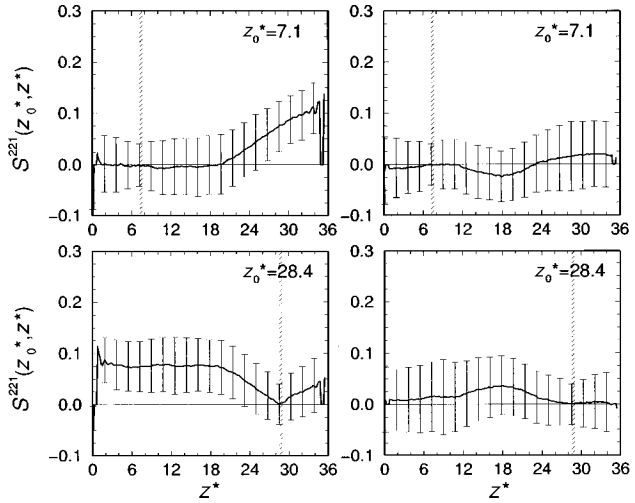

Fig. 5 Fluid–fluid chiral correlation $S^{221}(z_0^*, z^*)$ between molecules within slabs z^* and, respectively, $z_0^* = 7.1$ (top), $z_0^* = 28.4$ (bottom) for the sample at $T^* = 3.20$. The left-hand diagrams are those for the sample confined between a chiral ($c = -2$) and an achiral surface ($c = 0$), while those on the right are for a reference system confined between two achiral surfaces ($c = 0$). The reference higtogram bins at z_0^* are marked with a hatched line, and the root-mean-squared fluctuations are plotted every twenty histogram bins.

lation changes its sign as a consequence of a change in the handedness of the director twist θ as a function of z^*. Such behaviour would have been expected if the twist angle θ of the local director increased while moving apart from the chiral surface before relaxing to $\theta = 0°$. Such an effect would be detected in spite of the quite large fluctuation range, since the correlation functions for the chiral system are significantly different from the baseline behaviour provided by the reference simulation with two achiral surfaces, where these functions are close to zero all over the sample (Fig. 5).

To have an immediate grasp of the significance of the detailed analysis presented so far in terms of molecular organization, the structure of these fluid phases is visualized in Fig. 6. We show two snapshots of the confined fluid sample ($T^* = 4.0$ and $T^* = 3.2$) seen from the $-x$ direction. The particles at the left and right sides correspond to those of the chiral (green) and achiral (grey) surfaces respectively. The fluid particles are colour coded according to the twist angle θ, calculated as the angle between the y axis and the projection of $\hat{\boldsymbol{u}}_i$ on the xy plane. The central fluid region of the sample at $T^* = 4.0$ is isotropic (all colours are present). The extent of the twisted region (left portion of the sample) is small, in agreement with the conclusions drawn on the basis of the $S^{221}(z^*)$ functions. In the nematic sample ($T^* = 3.2$) the orientational behaviour is quite different and the molecules with a positive twist θ are the majority. Only in a small region close to the achiral surface (right portion of the sample) are both positive and negative molecular twists equally probable. The analyses of these pictorial representations support the conclusions drawn on the basis of the histograms of orientational correlation functions.

Conclusions

We have examined, with the help of computer simulations, the induction of a director twist from a planar surface covered by chiral molecules into a nematic. With the use of surface–fluid and fluid–fluid scalar and pseudoscalar orientational correlation functions we have shown that a twist of the local director with respect to the orientation of the chiral surface molecules is induced by the short-range chiral interactions. The local director twist has its maximum value nearest to the chiral surface. On lowering the temperature, the region with a

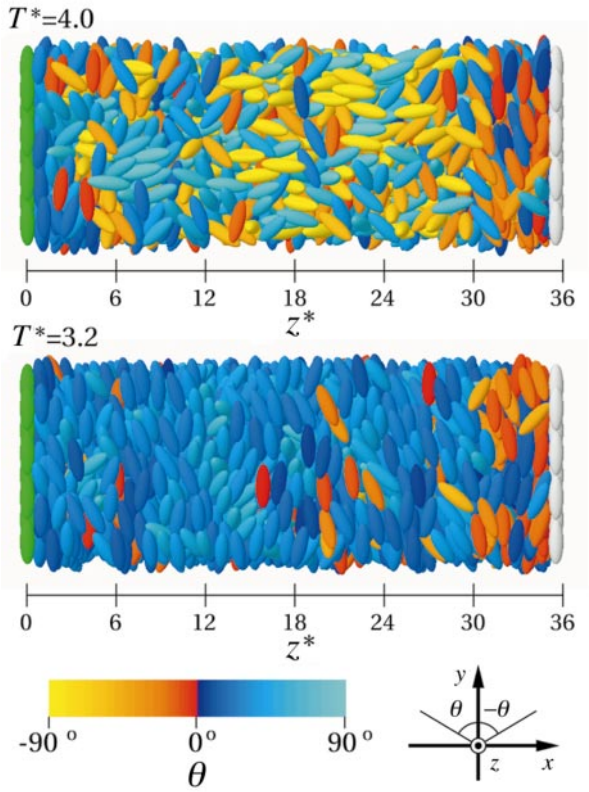

Fig. 6 Snapshots of two MC configurations at $T^* = 4.0$ (top) and $T^* = 3.2$ (bottom) as seen from the $-x$ direction. The fluid particles, represented here as uniaxial ellipsoids, are colour coded using the palette shown, according to the angle θ formed by the projection of their molecular axis $\hat{\boldsymbol{u}}_i$ on the xy plane with respect to y. The chiral (green) and achiral (grey) surface particles are shown on the left and right-hand sides.

twisted local director is extended up to large distances from the inducing surface deep inside the fluid phase, by the combined effect of short-range chiral surface–fluid interactions and long-range anisotropic correlations. In our case the director twist eventually relaxes smoothly to zero under the influence of the achiral counter-surface. Our results indicate that it is through the onset of long-range orientational correlations in the nematic phase that a twisted local director is conserved. The induction of a cholesteric phase by chiral particles in a nematic matrix could be explained by a superposition of such chiral distortions which sum up to the macroscopically observed helical structure, in agreement with de Gennes model.[2] In this case the induction and long-range conservation of the local director twist could be interpreted as a basic mechanism of the induction of a chiral nematic phase.

We thank the DAAD (Bonn), MURST and CNR (Rome) as well as University of Bologna for financial support and the Regionales Hochschulrechenzentrum Kaiserslautern and the Höchstleistungsrechenzentrum Jülich for generous allocation of computer time. R.B. and R.M. express their gratitude to the joint German–Italian Vigoni project for supporting essential exchange visits.

References

1 G. Friedel, *Ann. Phys.* (*Paris*), 1922, **18**, 273.
2 P. G. de Gennes and J. Prost, *The Physics of Liquid Crystals*, Oxford University Press, Oxford, 2nd edn., 1993, ch. 6.
3 L. D. Hayward and R. N. Totty, *Can. J. Chem.*, 1971, **49**, 624.
4 G. Briegleb, H-G. Kuball, K. Henschel and W. Euing, *Ber. Bunsen-Ges. Phys. Chem.*, 1972, **76**, 101.
5 H.-G. Kuball, B. Weiß, A. K. Beck and D. Seebach, *Helv. Chim. Acta*, 1997, **80**, 2507.
6 W. J. A. Goossens, *Mol. Cryst. Liq. Cryst.*, 1971, **12**, 237.

7 B. W. van der Meer, G. Vertogen, A. J. Dekker and J. G. J. Ypma, *J. Chem. Phys.*, 1976, **65**, 3935.
8 H-G. Kuball and H. Brüning, *Chirality*, 1997, **9**, 407.
9 J. G. Gay and B. J. Berne, *J. Chem. Phys.*, 1981, **74**, 3316.
10 R. Berardi, A. P. J. Emerson and C. Zannoni, *J. Chem. Soc., Faraday Trans.*, 1993, **89**, 4069.
11 D. J. Adams, G. R. Luckhurst and R. W. Phippen, *Mol. Phys.*, 1987, **61**, 1575.
12 M. K. Chalam, K. E. Gubbins, E. de Miguel and L. F. Rull, *Mol. Simul.*, 1991, **7**, 357.
13 E. de Miguel, L. F. Rull, M. K. Chalam, K. E. Gubbins and F. van Swol, *Mol. Phys.*, 1991, **72**, 593.
14 M. P. Allen and M. A. Warren, *Phys. Rev. Lett.*, 1997, **78**, 1291.
15 C. Zannoni, in *The Molecular Physics of Liquid Crystals*, ed. G. R. Luckhurst and G. W. Gray, Academic Press, London, 1979, ch. 9.
16 R. Memmer, H-G. Kuball and A. Schönhofer, *Liq. Cryst.*, 1993, **15**, 345.
17 A. J. Stone, *Mol. Phys.*, 1978, **36**, 241.
18 J. A. Barker and R. O. Watts, *Chem. Phys. Lett.*, 1969, **3**, 144.
19 M. P. Allen and A. J. Masters, *Mol. Phys.*, 1993, **79**, 277.
20 M. P. Allen, *Phys. Rev. E*, 1993, **47**, 4611.
21 R. Memmer, H-G. Kuball and A. Schönhofer, *Ber. Bunsen-Ges. Phys. Chem.*, 1993, **97**, 1193.

Paper 7/08446C; *Received* 24*th November*, 1997